Dyes and Pigments 95 (2012) 713–722

Contents lists available at SciVerse ScienceDirect

Dyes and Pigments

journal homepage: www.elsevier.com/locate/dyepig

Two-photon absorption properties of push–pull oxazolones derivatives

Catarina A.B. Rodrigues [a], Inês F.A. Mariz [b], Ermelinda M.S. Maçôas [b,*], Carlos A.M. Afonso [a], José M.G. Martinho [b]

[a] Research Institute for Medicines and Pharmaceutical Sciences (iMed.UL), Faculty of Pharmacy, University of Lisbon, Av. Prof. Gama Pinto, 1649-003 Lisbon, Portugal
[b] Centro de Química-Física Molecular and IN-Institute of Nanoscience and Nanothecnology, Instituto Superior Técnico, Av. Rovisco Pais, 1049-001 Lisboa, Portugal

ARTICLE INFO

Article history:
Received 24 April 2012
Received in revised form
12 June 2012
Accepted 13 June 2012
Available online 10 July 2012

Keywords:
Two-photon absorption
Fluorescence
Oxazolone
Solvatochromism
Nonlinear emission
Push-pull

ABSTRACT

New fluorescent oxazolone derivatives with high two-photon absorption cross-section were synthesized. Electron donor (phenyl, dimethylaniline and furanyl) and acceptor (nitrobenzene and ethenyl-phenyl-benzimidazol) groups have been appended to the methylene end of 4-(methylidene)-2-phenyl-1,3-oxazol-5(4H)-one in order to produce an highly conjugated π-system with push–pull geometry. The linear and nonlinear optical properties of the oxazolones have been determined. The compounds with a high charge transfer from the substituent group to the oxazolone ring have relatively high two-photon absorption cross-sections (80–100 GM). The best performing nonlinear fluorophore being the benzimidazol derivative with a two-photon absorption cross-section of 80 GM and a relatively high emission quantum yield, $\phi = 0.31$.

© 2012 Elsevier Ltd. All rights reserved.

1. Introduction

Two-photon absorbing fluorophores are compounds that emit light after absorbing simultaneously two photons that promote the transition of an electron from a lower energy level to a higher level. The absorbed photons are up-converted into emitted photons with twice the energy. These type of compounds have attracted high interest in the last decade due to their photochemical properties and subsequent wide range of applications such as microfabrication, data storage, photodynamic therapy, optical power limiting and sensors [1,2]. Many compounds with two-photon absorption (TPA) have been described in the literature [1,2]. Optimization of the TPA cross-section generally requires molecular structures of high complexity employing long synthetic procedures [1,2].

Oxazol-5-(4H)-ones (hereafter referred to as oxazolones) are small and simple molecules that have the general structure presented in Fig. 1a. Due to their numerous reactive sites, oxazolones have a wide range of applications in chemistry and biology [3,4]. Oxazolones are valuable precursors in the synthesis of non-natural aminoacids [5] and biological active heterocyclic molecules [3] which led to a great interest on different types of transformations to access highly substituted scaffolds [6–21].

One of the main issues regarding application of oxazolones is related to their poor photochemical stability. This issue can be circumvented in the solid phase because the photochemical decomposition due to ring-opening is strongly inhibited. In addition, the emission quantum yields of oxazolones with an exocyclic double bond at position 4 (Fig. 1b), also known as unsaturated oxazolones, are usually low. One of the factors determinant of the low quantum yield is the Z to E– geometrical isomerization. Encapsulation in the solid matrix prevents geometrical isomerization, thus increasing the radiative quantum yield. An interesting application of oxazolones in solid phase (dispersed in sol–gel and polymer matrices) is that of optical pH sensors [22–24].

With introduction of an exocyclic double bond at position 4 of the ring (Fig. 1b) the oxazolone gains a new reactivity in this position that allows the construction of interesting molecular structures [25–33]. This double bond also creates a highly conjugated π-system and subsequently new photophysical behaviour that makes oxazolones suitable for applications in photonics and electronics. Since the late 70's this conjugated system attracted the attention of several scientists and the influence of aryl substituents in the absorption and fluorescence of oxazolones have been extensively studied [34–37]. In 1995 the first observation of nonlinear optical behaviour of oxazolones trough second harmonic generation (SHG) [38] was reported. Since then a huge amount of studies regarding spectroscopy and nonlinear properties of oxazolones have been described [39–44]. One of these studies mentioned that oxazolones might show TPA characteristics [42].

---

* Corresponding author. Tel.: +351 218419218.
E-mail address: ermelinda.macoas@ist.utl.pt (E.M.S. Maçôas).

0143-7208/$ – see front matter © 2012 Elsevier Ltd. All rights reserved.
http://dx.doi.org/10.1016/j.dyepig.2012.06.005

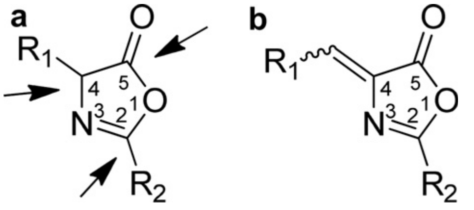

Fig. 1. a) General structure of oxazol-5-(4H)-ones and their reactive sites a, b) general structure of unsaturated oxazol-5-(4H)-ones.

Herein, we present the study of TPA properties of a set of push–pull compounds based on 4-(methylidene)-2-phenyl-1,3-oxazol-5(4H)-one easily synthesised by the well-known Erlenmeyer method [45,46]. The goal of this study is to understand the photophysics of a set of oxazolone derivatives with D-π-A and A-π-A arrangements in order to gain insight on the design of oxazolone derivatives with high two-photon absorption cross-section (σ_2) and acceptable fluorescence quantum yields (ϕ). These are properties that potentiate their application as labels in bioimaging, and as nonlinearly activated optical sensors. The nonlinearity of interaction with light is particularly advantageous when working in biological samples due to the intrinsic reduction of out of focus photobleaching and photodamage, and the greater penetration depth of the longer wavelengths used in multiphoton excitation [47]. In addition, the up-converted emission signal, usually in the visible range, is very efficiently separated from scattered excitation light in the infrared range. The main problem of multiphoton excitation relates to the high excitation powers required due to the low probability of the nonlinear absorption process (typically σ_2 values are $\sim 10^{-51}$–10^{-46} cm^{4}s while linear absorption cross-sections are $\sigma_1 \sim$ 10^{-19}–10^{-16} cm^2), which causes significant bleaching in the focal plane. The unwanted bleaching can be reduced by designing more efficient nonlinear fluorophores. Indeed, commercially available fluorophores used in bioimaging, which simultaneously show a high degree of selectivity toward specific cell organelles and biologically relevant molecules, have very low σ_2 values ($<$20 GM, 1 GM $= 10^{-50}$ cm^{4}s), with record high values around 200 GM reported for a few fluorophores [48]. The two-photon absorption is the most relevant nonlinear absorption process because it is a low order process and for stable fluorescent molecules it usually occurs under irradiation through the NIR optical window of biological samples.

2. Experimental and computational details

2.1. Material

All the reagents used were purchased from Aldrich or Merck and were used without further purification. The aldehyde used to synthesise compound VI was prepared accordingly to the described method [49]. The reaction evolution was followed by TLC using silica Merck Kieselgel 60 F254 plates, and revealed by ultraviolet light at 254 nm and 325 nm or stain solutions of phosphomolybdenum acid in ethanol.

2.2. Instrumentation

The compounds were characterized by NMR, in a Bruker Avance II 400 Ultrashield Plus, by elemental analysis performed at the Universidade Nova de Lisboa services, by infrared spectroscopy in a Shimadzu IRAffinity-1 FTIR spectrometer, using KBr platelets, by measuring the melting point in a Stuart SMP10 apparatus and by mass spectrometry in a quadrupole ion trap mass spectrometer Varian Inc. Palo Alto CA, USA, equipped with an ESI source. High Resolution mass spectra were obtained in a Finnigan FT/MS 2001 DT, FT-ICR/MS mass spectrometer, operating at EI positive mode.

The linear absorption spectra were recorded on a Shimadzu UV-3101PC UV–vis–NIR spectrophotometer. The emission spectra were recorded on a Horiba Jobin Yvon Fluorolog 3-22 Spectrofluorimeter. The solvatochromic shifts have been determined in spectroscopic grade solvents without further purification, degassing or drying. The solvents were chosen so has to span a wide range of dielectric constants without a significant change of the refractive index. In order of increasing dielectric constant, the solvents used were: benzene (Bz), toluene (Tol), chloroform (CF), diethyl ether (DE), methyl acetate (MA), ethyl acetate (EA), tetrahydrofuran (THF), dichloromethane (DCM), acetone (Ac), dimethylformamide (DMF), acetonitrile (ACN) and dimethylsulfoxide (DMSO).

The two-photon absorption spectra were measured by two-photon excited fluorescence using Rhodamine 6G (fluorescence quantum yield of 0.93, $\lambda_{em} = 500$–600 nm) [50] as a standard to account for collection efficiency and pulse characteristics. A modified setup that follows closely the one described by Xu and Webb [51] was used. In order to select a narrow bandwidth of emission wavelengths an H20Vis Jobin Yvon monochromator was placed at the entrance of a PMC-100-4 photomultiplyer tube (Becker and Hickl GmbH). The excitation source was a Ti:Sapphire laser (Tsunami BB, Spectra-Physics, 710–990 nm, 1.7 W, 100 s, 82 Mz). In general, solutions of 10 μM concentration in tetrahydrofuran (THF) were used. The TPA cross-sections of more challenging derivatives with low TPA values were evaluated in 2–0.7 mM concentrated THF solutions. The two-photon absorption cross-section was calculated from the relation:

$$\sigma_2 = \left(\frac{F_2}{\phi C n}\right)_{ox} \left(\frac{\phi C n \sigma_2}{F_2}\right)_{ref} \tag{1}$$

where F_2 stands for fluorescence intensity, ϕ is the one-photon excited fluorescence quantum yield, n refers to the refractive index of the solution, C is the concentration, and *ox* and *ref* are relative to the oxazolone derivatives and the Rhodamine 6G reference, respectively. The emission intensity dependence of the excitation power was checked to be quadratic at the excitation maximum for all the molecules studied.

The photostability of selected derivatives was tested under excitation with the spectrofluorimeter lamp (450 W Xe) through a slit width of 15 nm. The same conditions were used to study the photoisomerization.

2.3. Synthesis

The general method of synthesis of oxazol-5-(4H)-ones as been reported elsewhere [45,46] and it can be described as follows: all the reagents (aldehyde (1 eq.), hippuric acid (1.1eq.), sodium acetate (1 eq.) and acetic anhydride (2 eq.) were placed in a flask and stirred under 100–120 °C during 2 h. The mixture changed colour upon fusion of all the reagents. After cooling down to room temperature some methanol was added, the solid was filtered and washed with methanol. If further purification was needed some of the compounds were recrystallized in a suitable solvent. Details of the characterization of the oxazolone derivatives by NMR, IR, elemental analysis, melting point determination and mass spectrometry are given in the following sub-sections and additional structural spectra can be found in supplementary material.

2.3.1. (4Z)-4-Benzylidene-2-phenyloxazol-5(4H)-one (***I***)

Light yellow solid, yield: 64% (washed with methanol). M.p.: 166–167 °C. ^{1}H NMR (CDCl$_3$, 400 MHz) δ (ppm): 8.21 (td, $J = 8.4$, 1.7 Hz, 4H, 4× $C\underline{H}_{Ar}$), 7.66–7.58 (m, 1H, 1× $C\underline{H}_{Ar}$), 7.58–7.40 (m, 5H, 5× $C\underline{H}_{Ar}$), 7.26 (s, J = 1.4 Hz, 1H). ^{13}C NMR ($CDCl_3$, 101 MHz) δ (ppm) 167.64, 163.54, 133.52, 133.37, 133.27, 132.48, 131.79, 131.22, 128.95, 128.92, 128.39, 125.58. IR (KBr) ν: 1793.8, 1768.72, 1653, 1595.13, 1552.7, 1489.05, 1448.54, 1327.03, 1317.38, 1296.16, 1163.08, 983.7, 866.04, 767.67, 698.23, 686.66, 551.64 cm^{-1}. HRMS calc for $C_{16}H_{11}NO_2$: 249.078430, found: 249.077825. MS (ESI+) m/z calc for $[C_{16}H_{11}NO_2 + H]^+$: 250.07, found: 282.1 $[M + MeOH + Na]^+$, 250.1 $[M + H]^+$. Elemental Anal. Calcd. $C_{16}H_{11}NO_2$: % N, 5.62, % C, 77.10, % H, 4.45. Found: %N, 5.55; %C, 76.92; %H, 4.73.

*2.3.2. (4Z)-4-(4-nitrobenzylidene)-2-phenyloxazol-5(4H)-one (**II**)*

Yellow solid, yield: 66% (washed with methanol). M.p.: 242–244 °C (decomposition). ^{1}H NMR ($CDCl_3$, 400 MHz) δ (ppm) 8.35 (dd, J = 22.1, 8.7 Hz, 4H, 4× CHAr), 8.22 (d, J = 7.6 Hz, 2H, 2× CHAr), 7.68 (t, J = 7.2 Hz, 1H, 1× CHAr), 7.58 (t, J = 7.7 Hz, 2H, 2× CHAr), 7.24 (s, 1H, −C=CH−).^{13}C NMR ($CDCl_3$, 101 MHz) δ (ppm) 166.75, 165.66, 148.31, 139.39, 136.31, 134.26, 132.75, 129.17, 128.83, 127.56, 124.95, 123.96. IR (KBr), ν: 3103.46, 3066.82, 3043.67, 1797.66, 1761.01, 1654.92, 1641.42, 1598.99, 1579.7, 1556.55, 1519.91, 1489.05, 1452.4, 1413.82, 1361.74, 1344.38, 1325.1, 1296.16, 1240.23, 1224.8, 1163.08, 1109.07, 1093.64, 1070.49, 1001.06, 979.84, 894.97, 883.4, 867.97, 862.18, 848.68, 823.6, 777.31, 763.81, 746.45, 700.16, 684.73, 669.3 cm^{-1} MS (ESI+) m/z calc for [C16H10N2O4+1]: 295.26, found: 349.2 [M + MeOH + Na]+, 295.1 [M + H]+. Elemental Anal. Calcd. for C16H10N2O4: % N, 9.52, % C, 65.31, % H, 3.43. Found: %N, 9.23; %C, 65.28; %H, 3.64.

*2.3.3. (4Z)-4-(furan-2-ylmethylidene)-2-phenyloxazol-5(4H)-one (**III**)*

Brownish yellow solid, yield: 52% (washed with methanol). M.p.: 171–173 °C. ^{1}H NMR ($CDCl_3$, 400 MHz) δ (ppm) 8.14 (d, J = 7.5 Hz, 2H, 2× $C\underline{H}_{Ar}$), 7.67 (s, 1H, 1 ×$C\underline{H}_{Ar}$), 7.63–7.42 (m, 4H, 4 x$C\underline{H}_{Ar}$), 7.16 (s, 1H, −C=C$\underline{H}$−), 6.65 (s, 1H, 1× $C\underline{H}_{Ar}$).^{13}C NMR ($CDCl_3$,101 MHz) δ (ppm) 167.21, 163.10, 150.61, 146.77, 133.35, 130.50, 129.02, 128.38, 125.65, 120.28, 118.42, 113.92. IR (KBr) ν: 3012.81, 3039.81, 3062.96, 1789.94, 1753.29, 1649.14, 1629.85, 1598.99, 1558.48, 1490.97, 1465.9, 1452.4, 1328.95, 1296.16, 1232.51, 1157.29, 1024.2, 989.48, 941.26, 883.4, 862.18, 758.02, 700.16, 684.73, 592.15 cm^{-1}. MS (ESI+) m/z calc for $[C_{14}H_9NO_3+1]$: 240.06 found: 294.1 $[M + MeOH + Na]^+$, 273.1 $[M + MeOH]^+$, 240.1 $[M + H]^+$. Elemental Anal. Calcd. for $C_{14}H_9NO_3$ % N, 5.86, % C, 70.29, % H, 3.79. Found: %N, 5.73; %C, 70.19; %H, 3.88.

*2.3.4. (4Z)-4-[4-(dimethylamino)benzylidene]-2-phenyloxazol-5(4H)-one (**IV**)*

Bright orange needles. Yield: 45% (recristalized from ethyl acetate).M.p.: 218–219 °C. ^{1}H NMR ($CDCl_3$, 400 MHz) δ (ppm) 8.14 (d, J = 6.9 Hz, 4H, 4× $C\underline{H}_{Ar}$), 7.65–7.42 (m, 3H, 3×$C\underline{H}_{Ar}$), 7.20 (s, 1H,−C$\underline{H}$−C =), 6.75 (d, J = 8.8 Hz, 2H, 2× $C\underline{H}_{Ar}$), 3.09 (s, 6H, −N($C\underline{H}_3$)$_2$).^{13}C NMR ($CDCl_3$, 101 MHz) δ (ppm) 168.55, 160.58, 152.16, 134.86, 133.35, 132.30, 128.79, 128.33, 127.77, 126.34, 121.82, 111.82, 40.11 (N($\underline{C}H_3$)$_2$). IR (KBr) ν: 3080.32, 3035.96, 3022.45, 3005.1, 1784.15, 1762.94, 1647.21, 1606.7, 1595.13, 1581.63, 1568.13, 1529.55, 1490.97, 1448.54, 1375.25, 1323.17, 1296.16, 1195.87, 1161.15, 1126.43, 856.39, 813.96 cm^{-1}. HRMS calcd. for $C_{18}H_{16}N_2O_2$: 292.120629, found: 292.120841. MS (ESI+) m/z calc for $[C_{18}H_{16}N_2O_2+1]$: 293.12, found: 315.1 $[M + Na]^+$, 293.1 $[M + H]^+$. Elemental Anal. Calcd. for $C_{18}H_{16}N_2O_2$: % N, 9.88, % C, 73.95, % H, 5.52. Found: %N, 9.32; %C, 73.93; %H, 5.30.

*2.3.5. (4Z)-4-((E)-3-(4-(dimethylamino)phenyl)allylidene)-2-phenyloxazol-5(4H)-one (**V**)*

Dark red solid, yield: 55% (recrystallized from toluene), M.p.: 236 °C (decomposition). ^{1}H NMR ($CDCl_3$, 400 MHz) δ (ppm) 8.12 (d, J = 7.1 Hz, 2H, 2× $C\underline{H}_{Ar}$), 7.61–7.42 (m, 6H, 5× $C\underline{H}_{Ar\,+}$ −C=C$\underline{H}$−), 7.16 (d, J = 11.8 Hz, 1H, −C=C$\underline{H}$−), 7.07 (d, J = 15.3 Hz, 1H, −C=C$\underline{H}$−), 6.68 (d, J = 8.8 Hz, 2H, 2× $C\underline{H}_{Ar}$), 3.05 (s, 6H, −N($C\underline{H}_3$)$_2$). ^{13}C NMR ($CDCl_3$, 101 MHz) δ (ppm) 167.74, 160.95, 152.09, 146.18, 135.52, 132.90, 131.32, 130.61, 130.52, 129.29, 128.21, 127.87, 126.54, 124.46, 119.22, 112.36, 40.59 (N($\underline{C}H_3$)$_2$). IR (KBr) ν: 3035.96, 2897.08, 2858.51, 1770.65, 1641.42, 1608.63, 1589.34, 1575.84, 1550.77, 1523.76, 1490.97, 1450.47, 1371.39, 1325.1, 1300.02, 1276.88, 1224.8, 1163.08, 968.27, 867.97, 806.25, 723 14, 694.37 cm^{-1}. MS (ESI+) m/z calc for $[C_{20}H_{18}N_2O_2+1]$: 319.17, found: 351.2 $[M + Na]^+$, 319.2 $[M + H]^+$

*2.3.6. (4Z)-4-(4-((E)-2-(1H-benzo[d]imidazol-2-yl)vinyl)benzylidene)-2-phenyloxazol-5(4H)-one (**VI**)*

Light orange solid, yield: 52% (washed with methanol). M.p.: 233 °C (decomposition). ^{1}H NMR (DMSO, 400 MHz) δ (ppm) 8.38 (d, J = 8.3 Hz, 2H), 8.16 (d, J = 7.3 Hz, 2H), 7.84 (d, J = 8.3 Hz, 2H), 7.79–7.61 (m, 4H), 7.57 (dd, J = 5.9, 3.2 Hz, 2H), 7.39 (t, J = 8.2 Hz, 2H), 7.21 (dd, J = 6.0, 3.1 Hz, 2H). ^{13}C NMR (DMSO, 101 MHz) δ (ppm) 207.05, 167.35, 163.52, 151.04, 138.84, 134.22, 134.18, 133.87, 133.65, 133.33, 130.40, 129.85, 128.49, 128.02, 125.58, 122.83, 120.10. IR (KBr) ν: 3066.82, 3034.03, 2995.45, 1788.01, 1762.94, 1637.56, 1597.06, 1560.41, 1419.61, 1325.1, 1313.52, 1298.09, 1163.08, 983.7, 700.16 cm^{-1}. MS (ESI+) m/z calc for $[C_{25}H_{17}N_3O_2+1]$: 392.42, found: 424.3 $[M + MeOH]^+$, 392.2 $[M + H]^+$, Elemental Anal. Calcd. for $C_{25}H_{17}N_3O_2.2H_2O$: % N, 9.83, % C, 70.25, % H, 4.95. Found: %N, 9.74; %C, 69.79; %H, 5.40.

2.4. Computational methods

Calculations were done using Gaussian03 [52]. Ground state geometry optimizations were performed in vaccum at the B3LYP/6-31++g(2d,2p) level, and frequency calculations were used to ensure that a global minimum was reached. TDDFT calculations were done at the same level of approximation to estimate the Franck–Condon transition energies and the corresponding coefficients, transition dipole moments and oscillator strengths. The Onsager radius was calculated from the computed ground state molecular volume ($V_{mol} = 4\pi a^3/3$) using an increased density of points (keyword volume = tight) in the Monte Carlo integration as implemented in Gaussian03.

3. Discussion

A set of derivatives of 4-(methylidene)-2-phenyl-1,3-oxazol-5(4H)-one have been studied with different electron donor and acceptor substituents on the methylidene end (see Fig. 2). We anticipate that depending on the donor(D)/acceptor (A) strength of the substituents, the 2-phenyl-1,3-oxazol-5(4H)-one can act as an electron acceptor by accommodating an excess charge on the carbonyl group or as an electron donor with a charge deficient benzene ring. Derivatives **II** and **VI** are substituted with 4-nitrophenyl and 4[(E)-2-(1H-benzimidazol-2-yl)ethenyl] phenyl, which are typical electron acceptor groups in an A-π-A arrangement. Derivatives **III**, **IV** and **V** are substituted with furan-2-yl, and 4-(dimethylamino)phenyl either directly attached to the methylene end or separated by an ethylene bridge. These two molecules have a D-π-A arrangement. Compound **I** was prepared for the sake of completeness of the series. The asymmetric polarization induced by the presence of electron donor and electron acceptor groups in these π-electron conjugated molecules entails an extensive delocalization of the π-electron distribution, which is expected to favor their nonlinear interaction with light.

Table 1 summarizes relevant photophysical properties of the compounds, namely the maximum wavelength (λ_{max}) of one- and two-photon absorption (OPA and TPA), the maximum wavelength of one-photon induced emission (OPE), the fluorescence emission

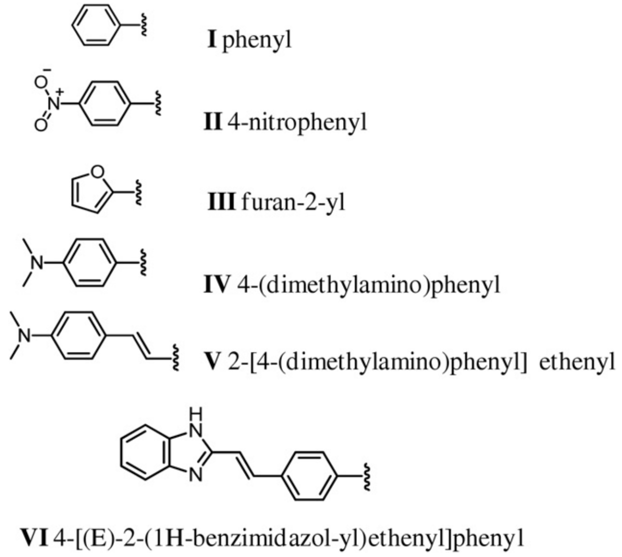

Fig. 2. 4-(methylidene)-2-phenyl-1,3-oxazol-5(4H)-one derivatives.

quantum yield (ϕ), and the two-photon absorption cross-section (σ_2, in GM units where 1 GM = 10^{-50} photons $cm^{-4}s^{-1}$). On the last column of Table 1 the values for the effective two-photon absorption cross-section are shown. These values, which are the product of the emission quantum yields with the TPA cross-sections, reflect the two-photon induced brightness of the molecules.

Based on the energy of the $S_0 \rightarrow S_1$ transition, the molecules in Table 1 can be separated into two sets: oxazolones **I**, **II** and **III** with higher energy transitions (360–390 nm) and oxazolones **IV**, **V** and **VI** with lower energy transitions (430–490 nm). This observation suggests that electronic delocalization in the ground state is more efficient for oxazolones **IV**, **V** and **VI**. Photostability tests show that, oxazolones **IV**, **V** and **VI,** unlike many of the previously studied oxazolone molecules [43], are stable at room temperature under excitation at maximum absorption wavelength (see supporting information). Excitation in the UV (330 nm) leads to very fast decomposition. Similarly, oxazolones **I**, **II** and **III** are photolabile under irradiation at the maximum absorption wavelength, which corresponds to excitation in the UV.

For all molecules, in the ground state the phenyloxazolone moiety and the substituent ring lay on the same plane. The extended conjugation in compounds **IV** and **V** leads to a nearly planar arrangement between the dimethylamine and the benzyl ring of the dimethylaniline group (≈4° off from planarity). The C–N bond distance is calculated to be 1.37 Å for both compounds, laying in between the typical bond distances between an aromatic carbon and an sp^2 (1.355 Å) and sp^3 (1.394 Å) nitrogen atom of an amine group [54]. With the exception of oxazolones **I** and **III**, all the studied molecules show a HOMO → LUMO transition with an appreciable charge transfer character, as shown in the isodensity surface of the frontier molecular orbital in Fig. 3. The charge is transferred from the phenyloxazolone moiety to the nitrophenyl group in compound **II**, while for compounds **IV**, **V** and **VI**, the charge is transferred in the reverse direction, from the dimethylamino or the benzimidazole groups to the phenyloxazolone terminus. Table 2 shows calculated properties relevant to UV–Vis absorption such as, transition energies, oscillator strength and transition dipole moments for the two lowest energy transitions. The molecular plane is the xy plane, with the *y* axis nearly aligned with the O=C….N molecular axis, and the positive direction of the *x* axis being towards the substituent group. Comparison of the experimental and calculated maximum absorption wavelength allows us to verify the accuracy of the calculations. The average difference between the theoretical and experimental values is less the 0.1 eV, which is acceptable, specially taking into consideration

Table 1
Photophysical properties[a] of substituted 4-(methylidene)-2-phenyl-1,3-oxazol-5(4H)-one solution in tetrahydrofuran.

Comp.	Substituent (R1)	λ_{max}^{OPA} (nm)	λ_{max}^{OPE} (nm)	λ_{max}^{TPA} (nm)	σ_2[b] (GM)	ϕ	$\sigma_2\phi$[b] (GM)
I	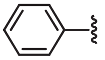	363	416	740	3	0.001	0.003
II	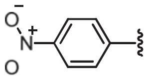	379	460	760	36	<0.001	0.011
III	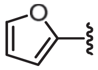	389	454	780	40	0.0003	0.012
IV	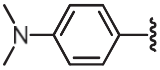	465	525	895	87	0.003	0.240
V	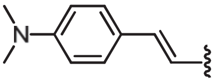	488	614	950	105	0.004	0.440
VI	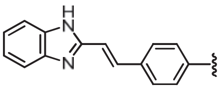	424	537	880	80	0.31	25.81

[a] OPA, OPE and TPA stand for one-photon absorption, one-photon emission and two-photon absorption, respectively.

[b] Two-photon absorption cross-section measured by two-photon induced emission using Rhodamine 6G in methanol as a standard ([50]) with quantum yield of 0.94 ([53]); 1 GM = 10^{-50} photons $cm^{-4}s^{-1}$. The estimated error limits for σ_2 are ±20% and for ϕ are less than ±10%.

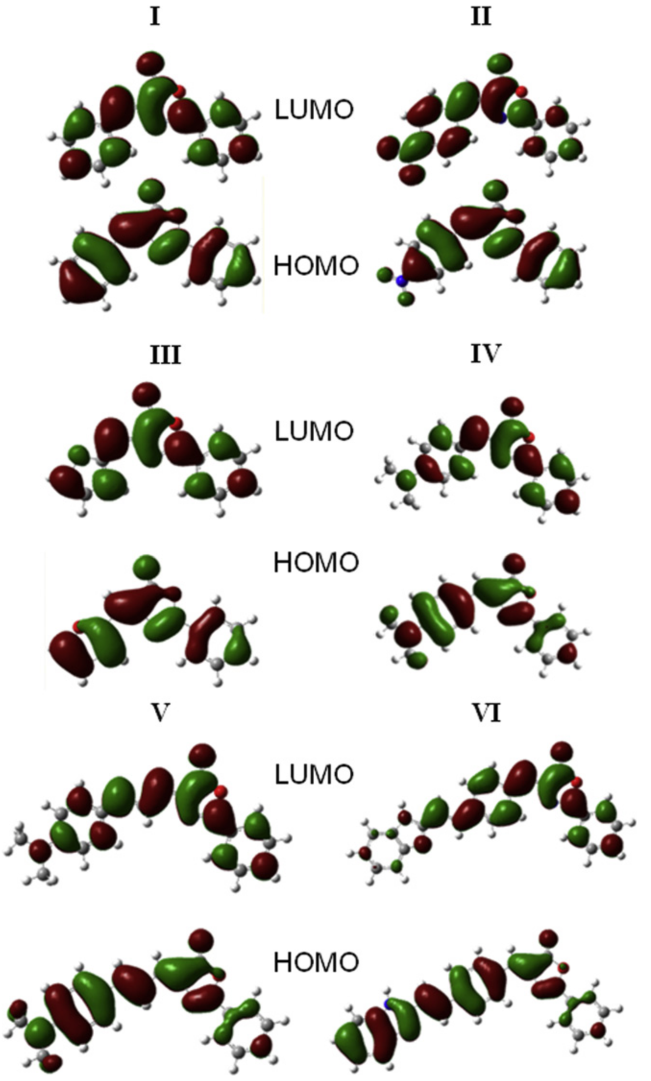

Fig. 3. Isodensity surfaces of the frontier molecular orbital of the oxazolone derivatives.

that the calculations were performed in vacuum. Nevertheless, it should be pointed out that the accuracy of the calculations is consistently worse for the molecules with a charge transfer excited state (**II**, **IV**, **V** and **VI**). Indeed, the limited accuracy in describing delocalized excited states (charge transfer states, valence state of molecules with extended π systems, Rydberg states) are known shortfalls in the performance of TDDFT calculations [55].

3.1. *Quantum yield*

Except for compound **VI** with $\phi = 0.31$, all compounds listed in Table 1 have a relatively low fluorescence quantum yields. The low quantum yields can be understood on the basis of an efficient nonradiative deactivation channel of the excess energy. Measurements of fluorescence lifetime of molecules **I**, **VI** and **V** confirm that the emission quantum yield is essentially determined by the non-radiative processes. The average fluorescence lifetime increases from a few picoseconds (3–10 ps) in **I** and **IV** to ≈ 0.9 ns in **VI**, which gives nonradiative decay rates decreasing in the order of 3×10^{11} (**I**), 9.5×10^{10} (**IV**) and $8.4 \times 10^{8}\ \mathrm{s}^{-1}$ (**V**). This nonradiative deactivation is well documented for molecule **I** and other ethynyl oxazolone derivatives as resulting from geometrical isomerization from the lowest energy isomer (the Z-isomer) to the less stable E-isomer taking place *via* a triplet state [56,57] Indeed, at room temperature, molecules **I**, **II** and **III** undergo isomerization when excited at their corresponding absorption maxima. As an illustrative example, Fig. 4 shows the excitation and emission spectra of the Z and E-isomers of molecule **II**. Excitation of the Z-isomer during 30 min at 379 nm leads to a red-shift of the absorption maximum by 15 nm due to the formation of the E-isomer, in good agreement with the calculation that predict the $S_0 \rightarrow S_1$ transition of the E-isomer to be shifted by 6 nm to lower energies, compared to the Z-isomer. Discrimination between the two isomers is more clear in emission, where emission of E-isomer appears red-shifted by about 70 nm ($\lambda_{\max} \approx 530$ nm) from that of the Z-isomer.

No isomerization was observed for molecules **IV**, **V** and **VI** upon excitation at their corresponding absorption maxima for more than 2 h. The absence of isomerization in these molecules can be understood on the basis of energetic considerations. As described above, oxazolones **IV**, **V** and **VI** have absorption maxima in the visible while oxazolones **I**, **II** and **III** have absorption maxima at considerably higher energies. Furthermore, we have observed that for molecule **I** decreasing the temperature up to 77 K increases the emission quantum yield. Even though isomerization is not expected at these low temperatures due to a solvent caging effect, the increased fluorescence quantum yield suggests that the triplet sate involved in the isomerization at higher temperatures is an activated state that is not efficiently populated at 77 K. Such an activated triplet is predicted for compounds **I** and **II** to be T_3 laying 3–17 nm above S_1. In **IV**, **V** and **VI** the T_3 triplets appears at 40–60 nm above S_1.

However, the absence of isomerization alone does not explain the low fluorescence quantum yields observed for compounds **IV** ($\phi = 0.003$) and **V** ($\phi = 0.004$), because the isomerization process was not observed in these molecules. Alternative, another non-radiative decay processes must be effective for these molecules. Indeed both molecules contain a dimethylamino donor (D) group and the oxazolone acceptor (A) group which are adequate to induce an efficient non-radiative decay channel due to formation of a twisted intramolecular charge transfer excited state. This process has been extensively studied in the analogous prototypical molecule of (4-dimethylamino)benzonitrile [58]. Further evidence of the intramolecular charge transfer from the dimethylamino group to the oxazolone ring come from the solvatochromic shifts in solvents of different polarity. We have studied the solvatochromic effect on the absorption and emission of oxazolones **IV**, **V** and **VI** using a set of solvents with increasing dielectric constant (from $\varepsilon = 2.28$ in Bz to $\varepsilon = 48.9$ in DMSO) and approximately constant refractive indexes (from $n = 1.50$ in Bz to $n = 1.34$ in ACN). Fig. 5 shows the sovatochromic effect on the absorption and emission spectra of oxazolones **IV**, **V** and **VI** for a reduced set of solvents.

Both the absorption and emission spectrum of oxazolone **IV** and **V** show a modest red-shift with increasing orientation polarization function (eq. (2)) whereas for oxazolone **VI** only in emission are appreciable solvatochromic shifts observed. The difference in the trend observed in the absorption spectra is readily understood on the basis of their respective ground state static dipole moment. The shift for the absorption and emission maxima are shown to be related to the ground and excited state dipole moments [59]:

$$\Delta f = \frac{(\varepsilon - 1)}{2\varepsilon + 1} - \frac{(n^2 - 1)}{2n^2 + 1} \tag{2}$$

$$\Delta\tilde{\nu}_{abs} = -\frac{2}{hca^3}\vec{\mu}_{00}(\vec{\mu}_{11} - \vec{\mu}_{00})\Delta f + c \tag{3}$$

$$\Delta\tilde{\nu}_{em} = -\frac{2}{hca^3}\vec{\mu}_{11}\left(\vec{\mu}_{11} - \vec{\mu}_{00}\right)\Delta f + c \tag{4}$$

Table 2
UV–Vis absorption properties (experimental in THF and calculated at TD-DFT level in vacuo).

Comp.	Exp. λ_{max} (nm)	Calc.						
		Transition energies (nm)	Oscillator strength	Transition dipole moment μ_{f0}			Orbitals	Coefficients
				x	y	z		
I	363	378	0.8577	−3.2480	−0.3346	0.0000	HOMO → LUMO	0.61913
		325	0.0003	0.0000	0.0000	−0.0523	HOMO-4 → LUMO	0.69305
II	379	409	0.8716	3.4246	−0.1190	0.0000	HOMO → LUMO	0.62602
		343	0.0002	−0.0003	0.0001	−0.0434	HOMO-4 → LUMO	0.67373
							HOMO-4 → LUMO+1	0.12908
III	389	398	0.7979	−3.1420	0.7640	0.0000	HOMO → LUMO	0.60329
		324	0.0003	0.0006	0.0000	−0.0580	HOMO-3 → LUMO	0.69322
IV	465	434	0.9410	3.6550	−0.2873	0.0074	HOMO → LUMO	0.62070
		320	0.1496	−1.2502	0.1102	−0.0087	HOMO → LUMO+1	0.48699
							HOMO-1 → LUMO	0.46746
							HOMO-5→LUMO	0.10523
V	488	467	1.3992	4.6302	−0.2026	0.0090	HOMO → LUMO	0.60939
		353	0.1563	−1.3398	−0.1514	−0.0049	HOMO-1 → LUMO	0.52610
							HOMO→LUMO+1	−0.41181
							HOMO → LUMO+4	−0.10420
							HOMO-5 → LUMO	−0.10153
VI	424	490	1.4255	4.7916	−0.1390	0.0000	HOMO→LUMO	0.64260
		396	0.1821	−1.4881	−0.4018	0.0000	HOMO-1 → LUMO	0.63839
							HOMO-2 → LUMO	0.23413
							HOMO → LUMO+1	−0.11188

where $\vec{\mu}_{11}$ and $\vec{\mu}_{00}$ are the static dipole moment of the excited and ground state, respectively.

The ground state dipole moments calculated for oxazolones **IV** and **V** are 7.54 and 8.89 D, while that estimated for oxazolone **VI** is considerably lower (2.02 D). Consequently, the absorption spectrum of oxazolones **IV** and **V** are more sensitive to solvent polarity. The fact that the emission spectra of the three molecules show a noticeable red-shift with increasing solvent polarity indicates that their excited states have quite large dipole moments. Indeed, the excited state dipole moment estimated on the basis of the slope of the $\Delta\tilde{\nu}_{abs}$ as a function of Δf (eq. (3)) assuming that the ground state and the excited state dipole moments are co-linear and using the calculated Onsager radius are 13 ± 3, 14 ± 4 and 13 ± 5 D for oxazolones **IV**, **V** and **VI** (Table 3 shows a list of the parameters used in the calculations). In the fitting procedure the less polar solvents (Bz and Tol) have been excluded from the correlation for two main reasons: i) both Bz and Tol have a large polarizability, and thus the dispersion contribution cannot be neglected as assumed in the derivation of eqs. (3) and (4); ii) the fluorescence of the compounds seems to indicate the formation of a charge transfer complex with the solvent (please see the fluorescence spectra of compounds **IV**, **V** and **VI** in Fig. 5). In order to evaluate if the excited state for absorption and emission is the same in each molecule, the excited state dipole moments can also be calculated from the slope of the $\Delta\tilde{\nu}_{em}$ as a function of Δf (eq. (4)), again assuming collinear dipole moments and using the calculated ground state dipole moment. This approach gives excited state dipole moments of 14 ± 1, 16 ± 1 and 15.4 ± 0.9 D for oxazolones **IV**, **V**, and **VI**, respectively. Since both approaches give, within our experimental error, equal excited state dipole moments, we can conclude that the same excited state is involved in absorption and emission. It should be noted that for compound **VI** the dipole moment of the ground and excited state are anti-parallel, as indicated by the negative $\Delta\tilde{\nu}_{abs}/\Delta f$ and positive $\Delta\tilde{\nu}_{em}/\Delta f$ in Table 3.

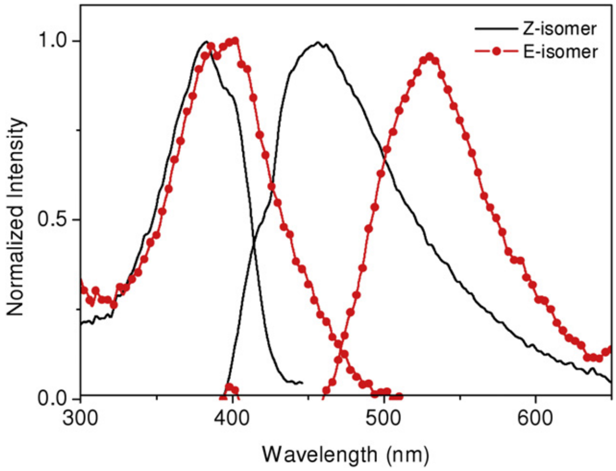

Fig. 4. Excitation and emission spectra of Z and E-isomers of molecule **II**. The excitation and emission spectra of the Z-isomer were recorded before irradiation by collecting emission at $\lambda_{em} = 460$ nm and upon excitation at $\lambda_{exc} = 379$ nm, respectively. The excitation spectrum of the E-isomer was recorded after 30 min of irradiation at 379 nm collecting emission at $\lambda_{em} = 520$ nm, while its emission spectrum was obtained by deconvolution of the emission spectra of the photostationary state in the E and Z isomer components.

Once it was established that the emissive state is populated *via* direct excitation from the ground state we can safely use the Stokes shifts to evaluate the dipole moment change exclusively based on experimental data using the Lippert–Mataga equation:

$$\Delta\tilde{\nu}_{SS} = \frac{2}{hca^3}(\mu_{11} - \mu_{00})^2\Delta f + c \tag{5}$$

where $\Delta\tilde{\nu}_{SS}$ refers to the change in the stokes shift. The plot of the Stokes shift versus the orientation polarization function, Δf, is shown in Fig. 6. It is noteworthy that in this figure the Bz and Tol points obey the linear correlation though they have not been considered in the fitting due to difficulty in discriminating the position of the absorption maxima corresponding to the uncomplexed molecules. This probably occurs because the Stokes shift is essentially determined by the emission shift and the emission maxima coincides with emission from the uncomplexed molecules. The ratio between eqs. (3) and (4) allows us to estimate the ground state dipole moment from the solvatochromic shifts. This gives ground state dipole moments (5 ± 3 D (**IV**), 5 ± 4 D (**V**) and 1.5 ± 0.6 D (**VI**)) in good agreement with those obtained from the electronic structure calculations (7.5 D (**IV**), 8.9 D (**V**) and 2.0 (**VI**) D. Eq. (5)

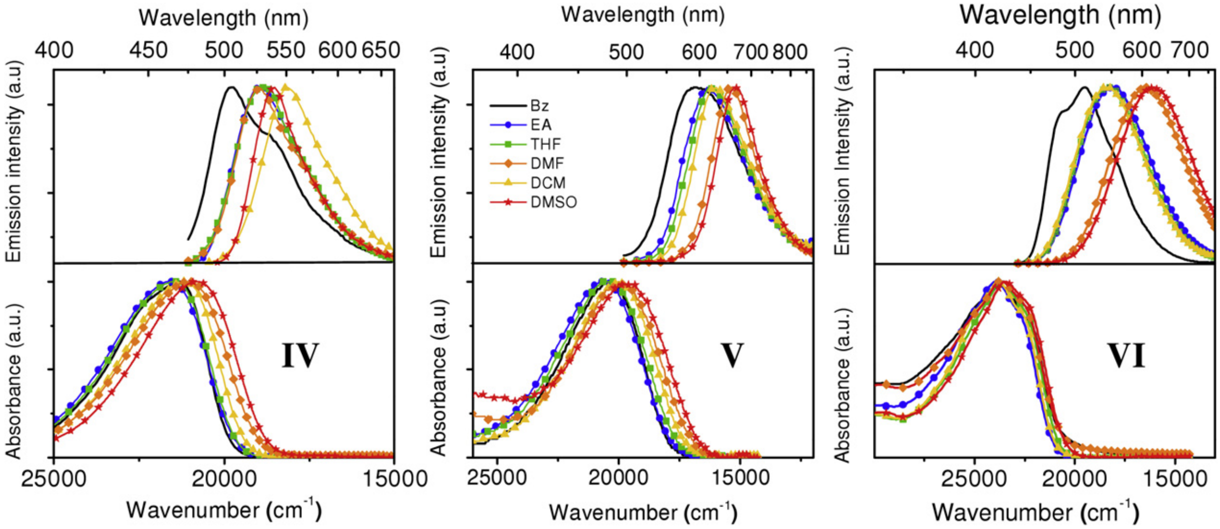

Fig. 5. Solvatochromic effects on the linear absorption and emission spectra of oxazolones **IV**, **V** and **VI**. The solvent abbreviations correspond to: Bz, benzene; EA, ethyl acetate; THF, tetrahydrofuran; DMF, dimethylformamide; DCM, dichloromethane and DMSO, dimethylsulfoxide.

allows us to estimate the difference between the permanent dipole moments to be 7.0 ± 0.7 D (**IV**), 7.8 ± 0.6 D (**V**) and 15 ± 1 D (**VI**). Note that the difference between the static dipole moments for **VI** ($\Delta\mu_{SS} = 15 \pm 1$ D) is higher that the excited state dipole moment ($\mu_{11} = 13.7 \pm 0.9$ D) because the ground and excited state dipole moments are anti-parallel. The charge transfer character of the $S_0 \rightarrow S_1$ electronic transition is stronger for the **VI** derivative.

Fig. 6 shows that the magnitude of the Stokes shifts increases from oxazolone **IV** to **V** and **VI** implying that there is an extensive structural rearrangement of the solvent molecules from the Franck–Condon geometry reached upon absorption to attain the relaxed emissive charge transfer state. This structural relaxation implies a solute-solvent coupling that could lead to an effective nonradiative energy relaxation, and for low emission quantum yield. The reason for oxazolone **VI** to have a much higher quantum yield than oxazolones **IV** and **V** remains unclear.

3.2. Two-photon absorption

Compound **I**, with a phenyl substituent is the one with the lowest TPA cross-section (3 GM). All the other derivatives have TPA cross-section ranging from ≈40 to 100 GM (Table 1), which are comparable with those of commercial TPA dyes. Derivatives **II** and **III**, with TPA cross-sections of ≈40 GM, have exceedingly low emission quantum yields to be of any use as fluorescent labels in 3D-imaging. Alternatively, nonlinear absorption materials with low emission quantum yields have been used in optical power limiting applications. The oxazolone derivatives with the higher TPA cross-section have either strong donor groups (**IV** and **V**) or a relatively mild acceptor substituent (**VI**), which transfer electron density to the oxazolone ring upon excitation. These three derivatives have at least one order of magnitude high effective TPA cross-section ($\sigma_2.\phi$) than the other studied derivatives (Table 1). The linear (OPA) and two-photon (TPA) absorption and fluorescence of oxazolones **IV**, **V** and **VI** in THF are shown in Fig. 7. The emission spectra are insensitive to the nature of the excitation process. As discussed above, the broad and unstructured emission bands are characteristic of intramolecular charge transfer in the excited state. As a result of the charge transfer nature of the Franck–Condon excited state, molecules **IV**, **V** and **VI** have the higher TPA cross-sections (87, 105 and 80 GM, respectively). For oxazolones **IV** and **V** the TPA spectra can be overlapped with the OPA spectra using for the TPA spectra an energy scale factor that is exactly twice the wavelength of the OPA spectra. In contrast, oxazolone **VI** has two TPA maxima (740 and 880 nm) underneath the apparently unstructured OPA absorption centered at 424 nm.

For polar unsymmetrical molecules with either parallel or antiparallel dipole moments, the two-photon absorption cross-section is generally well described within the framework of a two-level system as follows [60]:

$$\sigma_2(\nu) = \frac{2(2\pi L)^4}{5(hcn)^2}(\mu_{11} - \mu_{00})^2\mu_{10}^2 g(2\nu) \qquad (6)$$

where L is the Lorentzian local field factor ($L = (n^2+2)/3$), μ_{10} is the transition dipole moment and $g(2\nu)$ is the normalized TPA line

Table 3
Measured spectroscopic data and calculated parameters relevant for the estimation of permanent dipole moments from solvatochromic effects are listed together with the estimated dipole moments and TPA cross-sections.

Comp.	$S_0 \rightarrow S_1$ exp (nm)	$\varepsilon_{max} \times 10^4$ (cm^{-1}/M^{-1})	a calc (Å)	$\Delta\nu_{abs}/\Delta f$ (cm^{-1})	$\Delta\nu_{em}/\Delta f$ (cm^{-1})	$\Delta\nu_{SS}/\Delta f$ (cm^{-1})	$\Delta\mu_{SS}$[a] (D)	μ_{11}[b] (D)	$\sigma_{2\ SS}$[c] (GM)	$\sigma_{2\ TPEF}$[d] (GM)
VI	465	5.41	4.52	−4138	−9504	5366	7.0 ± 0.7	12 ± 6	75	87
V	488	4.74	4.59	−4270	−10586	6315	7.8 ± 0.6	13 ± 5	85	105
VI	424	4.75	4.87	1978	−18035	20013	15 ± 1	14 ± 3	287	80

[a] $\Delta\mu_{ss}$ is the permanent dipole moment change calculated from $\Delta\nu_{SS}/\Delta f$ and equation (5).

[b] μ_{11} is the excited state dipole moment extracted from $\Delta\nu_{SS}/\Delta f$ and $\Delta\nu_{em}/\Delta f$ according to equations (4) and (5).

[c] $\sigma_{2\ SS}$ is the TPA cross-section calculated according to equation (7) with an estimated error of ±20%.

[d] $\sigma_{2\ TPEF}$ is the measured absorption cross-section with an estimated error of ±20%.

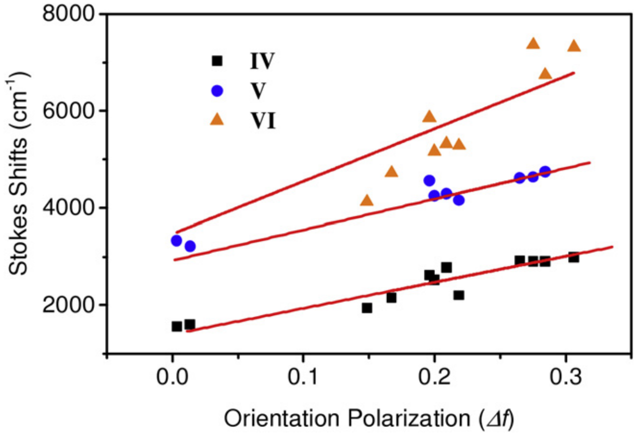

Fig. 6. Stokes shift as a function of the solvent orientation polarization showing the fitting of the experimental data points to eq. (5) (straight line). For each compound. the two experimental points with Δ*f* close to zero correspond to Bz and Tol and have not been considered in the fitting to eq. (5).

shape function. Assuming that the TPA line shape can be approximated by the OPA line shape it is possible to describe the TPA cross-section based on linear spectroscopic properties such as the dipole moment change, the extinction coefficient and the frequency of the maximum of the OPA band, as follows [60]:

$$\sigma_2(\nu) = \frac{12}{5}\frac{ln10\pi10^3}{N_A hc^2}\frac{L^4}{n^2}\frac{\varepsilon_{10(\nu)}}{\tilde{\nu}_{10}}(\mu_{11}-\mu_{00})^2 \tag{7}$$

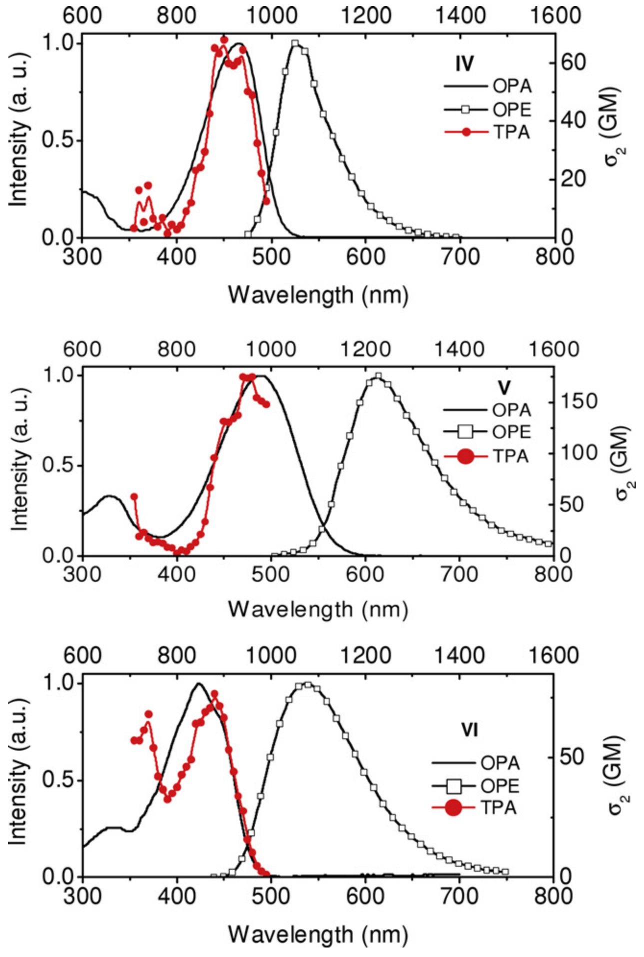

Fig. 7. Linear absorption and emission spectra and two-photon absorption spectra of oxazolones **IV V** and **VI** in THF.

In deriving this equation it was assumed that $\mu_{10}^2 g(2\nu)$ can be approximated by [60]:

$$\mu_{10}^2 g(2\nu) = \mu_{10}^2 g\left(\tilde{\nu}_{10}\right) = \frac{3\times10^3 ln10hc\varepsilon\left(\tilde{\nu}_{10}\right)n}{(2\pi)^3 N_A\tilde{\nu}_{10}L^2} \tag{8}$$

Thus, the dipole moment differences extracted from the Stokes shifts can be used to estimate two-photon absorption cross-section for this set of oxazolones. This approach was applied only to molecules **IV**, **V** and **VI** due to their higher TPA cross-section. Molecules **II** and **III** have exceedingly low emission quantum yields to allow for an accurate analysis of the solvatochromic shifts and molecule **I** has both low emission quantum yields and low TPA cross-section. The values obtained for the oxazolones **VI** and **V** using the spectroscopic data in Table 3 were 75 and 85 GM, which are in good agreement with the experimentally determined values of 87 and 105 GM. These values show that, even though increasing the conjugation length is a well-known strategy to increase the TPA cross-section [1], this effect is quite modest for the two dimethylaniline derivatives in this study. The experimental maximum obtained for oxazolone **VI** (80 GM) is equal to those of oxazolones **IV** and **V**. Conversely, the estimated value for the TPA of oxazolone **VI** on the basis of the linear spectroscopic properties is significantly higher than the measured one (287 GM). This discrepancy cannot be accounted for based on the approximation of the two-photon absorption line shape by that of the one-photon absorption. Comparison of the TPA and OPA spectra in Fig. 7 shows that the strongest band in the TPA spectra is considerably narrower than the strongest OPA band. The maximum of the normalized line shape function for the TPA is roughly three times higher than that of the OPA band. Thus a more accurate prediction of the TPA cross-section for oxazolone **VI** based on the TPA line shape function would actually be larger than the value on Table 3.

Similar discrepancies have been reported before by Rebane *et al.* and explained in terms of a molecular point dipole that is displaced from the center of the molecule [61], which is obviously the case for the studied oxazolone derivatives. The measured two-photon absorption cross-section does not depend on the exact location of the dipole moment due to the fact that the radiation wavelength is much larger than the molecular dimensions, thus the TPA cross-section is well defined by a point dipole approximation. Conversely the solvatochromic shifts do depend on interaction of the solute molecule with its immediate surroundings so that a displacement of the molecular dipole from the center of the molecule would lead to increased interaction energy. Thus, the dipole moments estimated from the solvatochromic shift could be overestimated leading also to an overestimation of the TPA cross-section. In the **IV** and **V** derivatives, the overestimation of the dipole moments seem to cancel out in the dipole moment difference, while in derivative **VI** the overestimation remains due to the fact that the ground state dipole moment is in fact small.

The additional shorter wavelength band in the TPA spectrum of oxazolone **VI** (740 nm) is assigned to a biphotonic transition to a higher energy singlet state. An S_2 state is predicted by the TD-DFT calculation to lay 93 nm above in energy from the S_1 state (Table 2). This prediction agrees well with the 70 nm estimated from the difference between the band maxima observed in TPA spectrum ($\lambda_{S1}^{OPA}-\lambda_{S2}^{OPA} = \lambda_{S1}^{TPA}/2-\lambda_{S2}^{TPA}/2$). The dominant transition is a HOMO-1 → LUMO transition that involves also some degree of charge transfer from the benzimidazole unit to the oxazolone terminus. The much weaker oscillator strength associated with this transition (almost one order of magnitude lower than the $S_0 \rightarrow S_1$ transition (see Table 2)) precludes its observation in the OPA spectra. Similar $S_0 \rightarrow S_2$ transitions are observed in the TPA spectrum of oxazolones **V** (730 nm), but with much weaker TPA cross-sections (14 GM).

The benzoimidazol derivative (**VI**) is by far the best performing molecule as a two-photon activated fluorophore, given the much higher quantum yield (Table 1). The effective TPA cross-section for oxazolone **VI** (25 GM) is almost two orders of magnitude higher that of oxazolones **IV** and **V** (0.24 and 0.44 GM, respectively). The value of the effective TPA cross-section of oxazolone **VI** is comparable to commercially available fluorophores like Fluorescein (60 GM), Rhodamine 6G (120 GM) or Rhodamine B (135 GM).

4. Conclusions

A set of push–pull molecules with either D-π-A or A-π-A arrangements have been synthesized based on the 2-phenyl-1,3-oxazol-5(4H)-one unit aiming at preparing stable oxazolone based fluorophores with appreciable nonlinear excitation. Their linear and nonlinear photophysical properties relevant to evaluation of the two-photon absorption cross-section have been characterized. The TPA cross-sections were estimated using two different approaches: (1) from the two-photon excited fluorescence and (2) calculated within a two-level approximation from the transition dipole moments and the changes between the permanent dipole moment extracted from linear spectroscopic data. Electronic structure allowed for a deeper insight into the nature of the relevant electronic transitions. The highest TPA cross-sections were estimated between 80 and 100 GM either for oxazolone derivatives with strong electron donating groups (dimethylamine) or mild electron accepting groups (benzoimidazol) that actually behave as electron donors with respect to the oxazolone ring. Thus, in this set of molecules the nonlinear interaction is favored by an efficient charge transfer from the substituent group to the oxazolone ring. Nevertheless, the dimethylamine and furanyl derivatives have extremely low quantum yields thus precluding their use as nonlinear fluorophores. Alternatively their nonlinear response could be relevant in optical power limiting applications. The best performing nonlinear fluorophore was the benzoimidazol derivative with a TPA cross-section of 80 GM and an emission quantum yield of 0.31. The results from this study will guide our future work on the oxazolone derivatives as a two-photon absorption fluorophores.

Acknowledgment

The authors thank the FCT-Fundação para a Ciência e a Tecnlogia for financial support (project PTDC/CTM-POL/114367/2009, PhD grant: SFRH/BD/48145/2008 and post-doc grant: SFRH/BPD/75782/2011)

Appendix A. Supplementary material

Supplementary material associated with this article can be found, in the online version, at http://dx.doi.org/10.1016/j.dyepig.2012.06.005.

References

[1] He GS, Tan L-S, Zheng Q, Prasad PN. Multiphoton absorbing materials: molecular designs, characterization, and applications. Chem Rev 2008;108:1245–330.

[2] Pawlicki M, Collins HA, Denning RG, Anderson HL. Two-photon absorption and the design of two-photon dyes. Angew Chem Int Ed 2009;48(18):3244–66.

[3] Fisk JS, Mosey RA, Tepe JJ. The diverse chemistry of oxazol-5-(4H)-ones. Chem Soc Rev 2007;36(9):1432–40.

[4] Alba ANR, Rios R. Oxazolones in organocatalysis, new tricks for an old reagent. Chem Asian J 2011;6(3):720–34.

[5] Mosey RA, Fisk JS, Tepe JJ. Stereoselective syntheses of quaternary substituted alpha-amino acids using oxazol-5-(4H)-ones. Tetrahedron-Asymmetry 2008;19(24):2755–62.

[6] Aleman J, Milelli A, Cabrera S, Reyes E, Jorgensen KA. Asymmetric 1,4-Addition of oxazolones to Nitroalkenes by Bifunctional cinchona Alkaloid Thiourea organocatalysts: synthesis of alpha, alpha-disubstituted alpha-amino acids. Chem Eur J 2008;14(35):10958–66.

[7] Cabrera S, Reyes E, Aleman J, Milelli A, Kobbelgaard S, Jorgensen KA. Organocatalytic asymmetric synthesis of alpha, alpha-disubstituted alpha-amino acids and derivatives. J Am Chem Soc 2008;130(36):12031–7.

[8] Uraguchi D, Ueki Y, Ooi T. Chiral Tetraaminophosphonium Carboxylate-catalyzed direct Mannich-type reaction. J Am Chem Soc 2008;130(43):14088.

[9] Dong SX, Liu XH, Chen XH, Mei F, Zhang YL, Gao B, et al. Chiral Bisguanidine-catalyzed inverse-electron-demand Hetero-Diels-Alder reaction of Chalcones with azlactones. J Am Chem Soc 2010;132(31):10650–1.

[10] Liu XD, Deng LJ, Jiang XX, Yan WJ, Liu CL, Wang R. Asymmetric Aza-Mannich addition of oxazolones to N-Tosyl Aldimines: synthesis of Chiral alpha-disubstituted alpha, beta-Diamino acids. Org Lett 2010;12(4):876–9.

[11] Weber M, Jautze S, Frey W, Peters R. Bispalladacycle-catalyzed bronsted acid/base-promoted asymmetric Tandem azlactone formation-Michael addition. J Am Chem Soc 2010;132(35):12222–5.

[12] Yang X, Lu GJ, Birman VB. Benzotetramisole-catalyzed dynamic kinetic resolution of azlactones. Org Lett 2010;12(4):892–5.

[13] Alba ANR, Calbet T, Font-Bardia M, Moyano A, Rios R. Alkylation of oxazolones and related heterocycles through an S(N)1 reaction. Eur J Org Chem 2011;(11):2053–6.

[14] De CK, Mittal N, Seidel D. A dual-catalysis approach to the asymmetric steglich rearrangement and catalytic enantioselective addition of o-acylated azlactones to isoquinolines. J Am Chem Soc 2011;133(42):16802–5.

[15] Di Giacomo M, Serra M, Brusasca M, Colombo L. Stereoselective Pd-catalyzed synthesis of quaternary alpha-D-C-Mannosyl-(S)-amino acids. J Org Chem 2011;76(13):5247–57.

[16] Dong SX, Liu XH, Zhang YL, Lin LL, Feng XM. Asymmetric synthesis of 3, 4-Diaminochroman-2-ones promoted by guanidine and bisguanidium salt. Org Lett 2011;13(19):5060–3.

[17] Lu GJ, Birman VB. Dynamic kinetic resolution of azlactones catalyzed by Chiral Bronsted acids. Org Lett 2011;13(3):356–8.

[18] Melhado AD, Amarante GW, Wang ZJ, Luparia M, Toste FD. Gold(I)-Catalyzed Diastereo- and enantioselective 1,3-Dipolar cycloaddition and Mannich reactions of azlactones. J Am Chem Soc 2011;133(10):3517–27.

[19] Terada M, Nii H. Highly Stereoselective 4+2 cycloaddition of azlactones to beta, gamma-unsaturated alpha-Ketoesters catalyzed by an axially Chiral Guanidine base. Chem Eur J 2011;17(6):1760–3.

[20] Truppo MD, Hughes G. Development of an improved immobilized CAL-B for the Enzymatic resolution of a key intermediate to Odanacatib. Org Proc Res Dev 2011;15(5):1033–5.

[21] Ying Y, Chai Z, Wang HF, Li P, Zheng CW, Zhao G, et al. Bifunctional cinchona alkaloids-catalyzed asymmetric 4+2 cycloaddition reaction of beta, gamma-unsaturated alpha-keto esters with oxazolones. Tetrahedron 2011;67(19):3337–42.

[22] Ertekin K, Alp S, Karapire C, Yenigül B, Henden E, İçli S. Fluorescence emission studies of an azlactone derivative embedded in polymer films: an optical sensor for pH measurements. J Photochem Photobiol A: Chem 2000;137(2–3):155–61.

[23] Ertekin K, Alp S, Yalcin I. Determination of pK(a) values of azlactone dyes in non-aqueous media. Dyes Pigment 2005;65(1):33–8.

[24] Ertekin K, Karapire C, Alp S, Yenigül B, Içli S. Photophysical and photochemical characteristics of an azlactone dye in sol-gel matrix; a new fluorescent pH indicator. Dyes Pigment 2003;56(2):125–33.

[25] Wu LX, Burgess K. Syntheses of highly fluorescent GFP-chromophore analogues. J Am Chem Soc 2008;130(12):4089–96.

[26] Misra NC, Ila H. 4-Bis(methylthio)methylene-2-phenyloxazol-5-one: versatile template for synthesis of 2-Phenyl-4,5-functionalized Oxazoles. J Org Chem 2010;75(15):5195–202.

[27] Amareshwar V, Mishra NC, Ila H. 2-Phenyl-4-bis(methylthio)methyleneoxazol-5-one: versatile template for diversity oriented synthesis of heterocycles. Org & Biomol Chem. 2011;9(16):5793–801.

[28] Baud MGJ, Leiser T, Meyer-Almes FJ, Fuchter MJ. New synthetic strategies towards psammaplin A, access to natural product analogues for biological evaluation. Org & Biomol Chem. 2011;9(3):659–62.

[29] Genady AR, Nakamura H. Amphiphilic allylation of arylidene-1,3-oxazol-5(4H)-one using bis-pi-allylpalladium complexes: an approach to synthesis of cyclohexyl and cyclohexenyl alpha-amino acids. Org Biomol Chem 2011;9(20):7180–9.

[30] Jiang H, Gschwend B, Albrecht L, Hansen SG, Jorgensen KA. Asymmetric Trienamine catalysis for the construction of structurally rigid cyclic alpha, alpha-disubstituted amino acid derivatives. Chem Eur J 2011;17(33):9032–6.

[31] Kaur H, Heapy AM, Brimble MA. The synthesis of dehydrotryptophan and dehydrotryptophan-containing peptides. Org Biomol Chem 2011;9(17):5897–907.

[32] Trost BM, Morris PJ. Palladium-catalyzed Diastereo- and enantioselective synthesis of substituted Cyclopentanes through a dynamic kinetic asymmetric

formal 3+2 -Cycloaddition of Vinyl Cyclopropanes and Alkylidene azlactones. Angew Chem Int Ed 2011;50(27):6167–70.

[33] Wang SL, Ding J, Jiang B, Gao Y, Tu SJ. Microwave-assisted solvent-dependent reaction: chemoselective synthesis of Quinoxalin-2(1H)-ones, Benzo d imidazoles and Dipeptides. Acs Comb Sci 2011;13(5):572–7.

[34] Krasovitskii BM, Lysova IV, Afanasiadi LS. Synthesis and spectral-Luminescence properties of 2-aryloxazole-5-ones. Khimiya Geterotsiklicheskikh Soedinenii 1978;(2):158–60.

[35] Krasovitskii BM, Lysova IV, Afanasiadi LS. Synthesis and spectral-lumine scence properties of 2- aryl- 4- benzylide ne-5-oxazolones. Chem Heterocyc Comp 1980;16(7):701–3.

[36] Krasovitskii BM, Lysova IV, Afanasiadi LS, Stryukov MB, Knyazhanskii MI, Vinetskaya YM. Luminescence properties of compounds containing both 2,5-diaryloxazole and 5-oxazole units. J Appl Spectrosc 1980;33(3):930–3.

[37] Krasovitskii BM, Lysova IV, Afanasiadi LS, Surov YN. Luminophores of the azlactone Series with Difluoromethylsulfonyl groups. Khimiya Geterotsiklicheskikh Soedinenii 1981;(12):1600–3.

[38] Kitazawa M, Higuchi R, Takasashi M, Wada T, Sasabe H. Novel molecular design for 2nd-Harmonic generation - Azlactone derivatives. J Phys Chem 1995;99(40):14784–92.

[39] Diaz JL, Villacampa B, Lopez-Calahorra F, Velasco D. Experimental and theoretical study of a new class of acceptor group in chromophores for nonlinear optics: 2-substituted 4-methylene-4H-oxazol-5-ones. Chem Mat 2002;14(5):2240–51.

[40] Song HC, Wen H, Li WM. Study on the second-order optical behavior of 4-(substituted-benzylidene)-2-phenyl-4H-oxazol-5-one. Spectrochim Acta A-Mol Biomol Spectrosc 2004;60(7):1587–91.

[41] Smokal V, Czaplicki R, Derkowska B, Krupka O, Kolendo A, Sahraoui B. Synthesis and study of nonlinear optical properties of oxazolone containing polymers. Synth Met 2007;157(18–20):708–12.

[42] Murthy YLN, Christopher V, Prasad UV, Bisht PB, Ramanaih DV, Kalanoor BS, et al. Synthesis and study of nonlinear optical properties of 4-substituted benzylidene-2-phenyl oxazol-5-ones by Z-scan technique. Synth Met 2010; 160(5–6):535–9.

[43] Derkowska B, Krupka O, Smokal V, Sahraoui B. Optical properties of oxazalone derivatives with and without DNA-CTMA. Opt Mater 2011;33(9):1429–33.

[44] Sun YF, Cui YP. The synthesis, structure and spectroscopic properties of novel oxazolone-, pyrazolone- and pyrazoline-containing heterocycle chromophores. Dyes Pigment 2009;81(1):27–34.

[45] Buck JS, Ide WS. Azlactone of alpha-benzoylamino-beta-(3,4-dimethoxyphenyl)-acrylic acid 2-phenyl-4-(3 ’, 4 ’-dimethoxybenzal)- oxazolone. Org Synth 1933;13:8–9.

[46] Acheson RM, Booth DA, Brettle R, Harris AM. The synthesis of some acylglycines and related Oxazolones. J Chem Soc 1960;(SEP):3457–61.

[47] König K. Multiphoton microscopy in life sciences. J Microsc 2000;200(2): 83–104.

[48] Diaspro A, Chirico G, Collini M. Two-photon fluorescence excitation and related techniques in biological microscopy. Quarter Rev Biophys 2005; 38(02):97–166.

[49] Huang ZL, Li N, Lei H, Qiu ZR, Wang HZ, Zhong ZP, et al. Two-photon induced blue fluorescent emission of heterocycle-based organic molecule. Chem Commun 2002;(20):2400–1.

[50] Makarov NS, Drobizhev M, Rebane A. Two-photon absorption standards in the 550-1600 nm excitation wavelength range. Opt Express 2008;16(6):4029–47.

[51] Xu C, Webb WW. Measurement of two-photon excitation cross sections of molecular fluorophores with data from 690 to 1050 nm. J Opt Soc Am B Opt Phys 1996;13(3):481–91.

[52] Frisch MJ, Trucks GW, Schlegel HB, Scuseria GE, Robb MA, Cheeseman JR, et al. Gaussian 03 RC. Wallingford CT: Gaussian, Inc.; 2004.

[53] Magde D, Wong R, Seybold PG. Fluorescence quantum yields and their relation to lifetimes of rhodamine 6G and fluorescein in nine solvents: Improved absolute standards for quantum yields. Photochem and Photology 2002; 75(4):327–34.

[54] Allen FH, Kennard O, Watson DG, Brammer L, Orpen AG, Taylor R. Tables of bond lengths determined by X-ray and neutron-diffraction .1. Bond lengths in organic-compounds. J Chem Soc-Perkin Trans 1987;2(12):S1–19.

[55] Dreuw A, Head-Gordon M. Single-reference ab initio methods for the calculation of excited states of large molecules. Chem Rev 2005;105(11):4009–37.

[56] Ullman EF, Baumann N. Unsaturated Lactone Photochemistry - Effect of wavelength and Sensitizer structure on selective population of specific excited states. J Am Chem Soc 1970;92(20):5892.

[57] Icli S, Doroshenko AO, Alp S, Abmanova NA, Egorova SI, Astley ST. Structure and luminescent properties of the 4-arylidene-2-aryl-5-oxazolones(azlactones) in solution and crystalline state. Spectrosc Lett 1999;32(4):553–69.

[58] Grabowski ZR, Rotkiewicz K, Rettig W. Structural changes accompanying intramolecular electron transfer: focus on twisted intramolecular charge-transfer states and structures. Chem Rev 2003;103(10):3899–4031.

[59] Lakowicz JR. Principles of fluorescence spectroscopy. 3rd ed. Singapore: Springer US; 2006.

[60] Drobizhev M, Meng FQ, Rebane A, Stepanenko Y, Nickel E, Spangler CW. Strong two-photon absorption in new asymmetrically substituted porphyrins: Interference between charge-transfer and intermediate-resonance pathways. J Phys Chem B 2006;110(20):9802–14.

[61] Rebane A, Drobizhev M, Makarov NS, Beuerman E, Haley JE, Douglas MK, et al. Relation between two-photon absorption and dipolar properties in a series of Fluorenyl-based chromophores with electron donating or electron withdrawing substituents. J Phys Chem A 2011;115(17):4255–62.